*Journal of Alloys and Compounds, 203* (1994) 15–22
*JALCOM 876*



# Characterization and magnetic properties of the new green-coloured $R_2BaCoO_5$ oxides (R ≡ Dy–Lu and Y)

J. Hernández-Velasco, A. Salinas-Sánchez, F. Fernández and R. Sáez-Puche*
*Departamento de Química Inorgánica, Facultad de Ciencias Químicas, Universidad Complutense de Madrid, 28040 Madrid (Spain)*

(Received May 16, 1993)

**Abstract**

New $R_2BaCoO_5$ compounds with R ≡ Dy, Er, Tm and Lu have been synthesized and characterized by X-ray powder diffraction. All of them are isostructural with the previously reported $R_2BaCoO_5$ where R ≡ Ho, Yb and Y. They crystallize in the $Sm_2BaCuO_5$ structural type and belong to the *Pnma* space group ($Z = 4$). The structural differences found between *Pnma*-$R_2BaCoO_5$ oxides and other related compounds are given. The magnetic properties of the whole family of oxides (R ≡ Dy–Lu and Y) have been studied from magnetic susceptibility measurements, showing the presence of three-dimensional antiferromagnetic interactions at low temperatures ($T_N < 5$ K) for most of these oxides.

## 1. Introduction

Two different structural types have been reported for the $R_2BaCoO_5$ oxides where R is a trivalent rare earth cation [1–3].

The brown-coloured oxides $R_2BaCoO_5$ (R ≡ Nd, Sm, Eu, Gd, Dy, Ho, Er and Tm) crystallize in the $Nd_2BaNiO_5$ structural type, with orthorhombic symmetry, space group *Immm*, $Z = 2$, showing as their main structural feature the presence of chains of corner-sharing $CoO_6$ flattened octahedra which run parallel to the *a* axis of the structure [1–6].

On the other hand, the green-coloured oxides $R_2BaCoO_5$ (R ≡ Ho, Yb and Y) crystallize in the $Sm_2BaCuO_5$ structural type, also with orthorhombic symmetry, but the *Pnma* space group, containing four formulae in the primitive cell. Although this structure is rather complex, it can be described as being based on a framework built up from $RO_7$ monocapped trigonal prisms that share a triangular face, giving rise to $R_2O_{11}$ units which form the skeleton of the structure. As can be seen in Fig. 1, the barium cations are located in the large holes of the structure surrounded by 11 oxygen atoms and it is possible to consider these $BaO_{11}$ polyhedra as tricapped distorted square prisms, while the cobalt ions form isolated $CoO_5$ distorted square pyramids.

Recently the existence of dimorphism has been reported for the $R_2BaCoO_5$ family of oxides with R ≡ Dy, Ho, Er and Tm [4–8]; as in the case of the $R_2BaNiO_5$ family with R ≡ Tm, Yb and Lu [9–12], both structural types, space groups *Immm* and *Pnma*, are present depending on the synthesis conditions used in the preparation.

The green *Pnma*-$R_2BaCoO_5$ phases are isostructural with the well-known $R_2BaCuO_5$ oxides [13–16], which are related to the high $T_c$ $RBa_2Cu_3O_{7-\delta}$ superconductors since they have been found as main impurities during the synthesis of the latter [17, 18]. Very recently the existence of antiferromagnetic ordering at 30 K has been shown in the $Cu^{2+}$ sublattice, which induces a subsequent ordering in the rare earth $R^{3+}$ sublattice at lower temperatures for most of these $R_2BaCuO_5$ compounds [19–23].

From these previous results on similar systems it would seem interesting to study the magnetic properties of the isostructural $R_2BaCoO_5$ phases, since current knowledge of these oxides is very sparse. Thus the purpose of this paper is the structural characterization by means of X-ray powder diffraction and the study of the magnetic properties from magnetic susceptibility measurements of the whole family of *Pnma*-$R_2BaCoO_5$ oxides (R ≡ Dy, Ho, Er, Tm, Yb, Lu and Y).

## 2. Experimental details

The *Pnma*-$R_2BaCoO_5$ oxides were prepared by solid state reaction from stoichiometric amounts of $R_2O_3$ (99.99%), $CoCO_3 \cdot nH_2O$ (99.999%) and $BaCO_3$ (A.R.

*Author to correspondence should be addressed.


*SSDI* 0925-8388(93)00876-Z

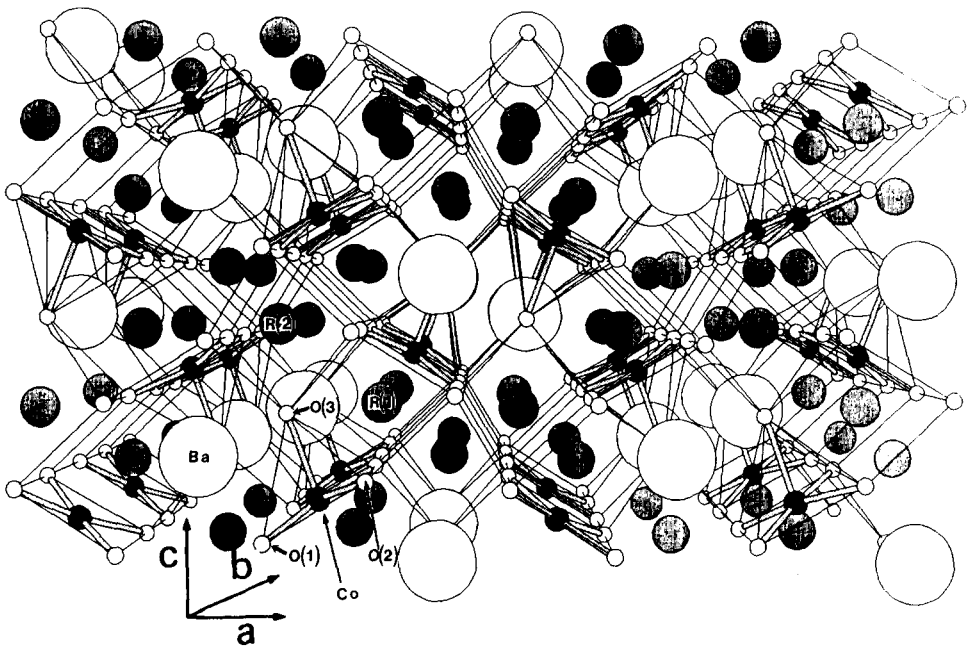


Fig. 1. Crystal structure of the *Pnma*-$R_2BaCoO_5$ oxides along the *b* axis showing the isolated $CoO_5$ square pyramids.

grade). The ground samples were heated in alumina crucibles under an argon flow, which is necessary owing to the instability of $Co^{2+}$ in air at high temperatures. Thermal treatments were carried out for 24 h at 1000–1300 °C, with several interruptions for re-grinding in order to enhance the homogeneity of the mixture.

X-Ray powder patterns were obtained using a Siemens Kristalloflex 810 diffractometer and D-500 goniometer equipped with a secondary graphite monochromator and Cu K$\alpha$ radiation. The data were collected by step scanning over an angular range of $10° < 2\theta < 120°$ in increments of 0.04° with a counting time of 15 s per step. All the data were analysed by the Rietveld method using the program FULLPROF [24]. Owing to the possibility of simultaneous fitting of various other phases, the $R_2O_3$ (cubic, space group $Ia\bar{3}$) and CoO (cubic, space group $Fm3m$) oxides were included as impurities in the profile refinements, since the background is a polynomial refinable function. The profile function used for describing the peak shape was a pseudo-Voigt type and no preferred orientations were taken into account.

The magnetic susceptibility measurements were performed in the temperature range 4.2–300 K with a fully automatic DSM8 magnetosusceptometer based on the Faraday method. The set-up was calibrated with $Hg[Co(SCN)_4]$, $Gd_2(SO_4)_3 \cdot 8H_2O$ and $NH_4Cr(SO_4)_2 \cdot 12H_2O$ as standards. The maximum magnetic field was 14 kG, with $HdH/dz \approx 24$ $kG^2$ $cm^{-1}$. The data were corrected for ionic diamagnetism by taking the values in e.m.u. $mol^{-1}$ of $-18\times10^{-6}$ for $R^{3+}$, $-32\times10^{-6}$ for $Ba^{2+}$, $-16\times10^{-6}$ for $O^{2-}$ and $-12\times10^{-6}$ for $Co^{2+}$ [25].

## 3. Results and discussion

### 3.1. Structural characterization

X-Ray powder diffraction data obtained for $R_2BaCoO_5$ (R ≡ Dy, Ho, Er, Tm, Yb, Lu and Y) oxides were indexed in the *Pnma* space group in all cases. As an example, in Fig. 2 the diffraction patterns of the new $Er_2BaCoO_5$ and $Tm_2BaCoO_5$ compounds are shown. The refinement was done using the starting positional values of the parameters reported by Mevs and Müller-Buschbaum [1, 3] for the isostructural $R_2BaCoO_5$ (R ≡ Y, Ho and Yb) oxides. The various diffraction data reveal that all the samples are almost but not quite single phases; however, the maximum weight fraction of impurity phases was only about 2% and this corresponds to the CoO and $R_2O_3$ oxides whose contributions to the intensities of the diffraction peaks were taken into account in the Rietveld refinement. The lattice parameters obtained for the various *Pnma*-$R_2BaCoO_5$ oxides are given in Table 1. It can be observed in Fig. 3, as was expected assuming the ionic model, that the lattice parameters *a*, *b* and *c* and the volume of the unit cell decrease linearly as a function of the rare earth ionic radius [26] in going from $Dy^{3+}$ to $Lu^{3+}$, which is concordant with the lanthanide contraction.

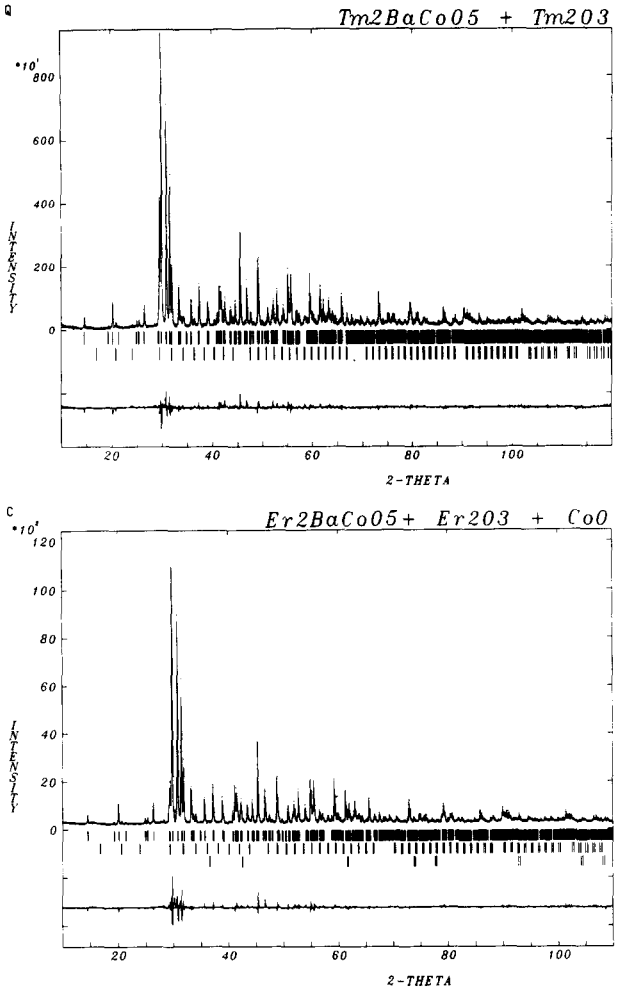


Fig. 2. X-Ray powder diffraction patterns of the new $Er_2BaCoO_5$ and $Tm_2BaCoO_5$ oxides. Points represent the experimental data and the solid curve is the calculated profile. A difference curve is plotted at the bottom. Vertical marks represent the positions of allowed Bragg reflections. The refinement was done taking into account the presence of small amounts of unreacted starting materials (see labels and text).

TABLE 1. Lattice parameters obtained for the *Pnma*-$R_2BaCoO_5$ oxides

| Compound | *a* (Å) | *b* (Å) | *c* (Å) |
|---|---|---|---|
| $Dy_2BaCoO_5$ | 12.3375(4) | 5.7250(2) | 7.0880(2) |
| $Ho_2BaCoO_5$ | 12.3000(7) | 5.7085(3) | 7.0680(4) |
| $Y_2BaCoO_5$ | 12.2945(9) | 5.7060(4) | 7.0696(5) |
| $Er_2BaCoO_5$ | 12.2568(2) | 5.6904(1) | 7.0415(2) |
| $Tm_2BaCoO_5$ | 12.2152(2) | 5.6739(1) | 7.0169(1) |
| $Yb_2BaCoO_5$ | 12.1712(3) | 5.6581(1) | 6.9977(2) |
| $Lu_2BaCoO_5$ | 12.1450(3) | 5.6456(1) | 6.9794(2) |

In Table 2 the refined positional parameters for the new *Pnma*-$R_2BaCoO_5$ oxides are listed (R ≡ Dy, Er, Tm and Lu). As was expected, the atomic coordinates obtained for each atom of the asymmetric unit are very close in all these oxides. Fairly good agreement is observed between our results and those previously reported from single-crystal X-ray data [1, 3] for the earlier-described *Pnma*-$R_2BaCoO_5$ (R ≡ Y, Ho and Yb) oxides.

In Table 3 the main interatomic distances are given for the Dy, Er, Tm and Lu compounds. A systematic variation in the lattice parameters and cell volume is observed in the *Pnma*-$R_2BaCoO_5$ family when the lanthanide cation is changed (Fig. 3), while the variation in the size of the cobalt pyramids ($CoO_5$) is less marked, the size remaining almost constant for the various oxides.

In this way, similar behaviour has been observed in the isostructural *Pnma*-$R_2BaCuO_5$ compounds [27], but in the case of the $CoO_5$ pyramid the distortion is very different compared with other $CuO_5$ and $NiO_5$ pyramids present in related oxides. In the case of the $R_2BaCuO_5$ compounds the Cu–O(3) bond length, which is the distance to the apex of the pyramid, is about 11% larger than the other four bond lengths [27], while in the so-called "blue phases" $R_2Cu_2O_5$ the axial Cu–O distance is about 40% larger than the basal plane Cu–O distances [28]. Also, in the superconducting phases $RBa_2Cu_3O_{7-\delta}$ the coordination pyramid is considerably more elongated than in the "green phases" [29]. In contrast, in the isostructural *Pnma*-$R_2BaNiO_5$ oxides the $NiO_5$ pyramids are flattened, Ni–O(3) being the shortest distance, about 2% smaller than the others [11]. In the present case the situation is quite different, because in the *Pnma*-$R_2BaCoO_5$ oxides the basal plane of the flattened $CoO_5$ pyramid is the most distorted compared with all the mentioned families of oxides. For example, in the isostructural $Yb_2BaNiO_5$ and $Yb_2BaCuO_5$ oxides these distances are Ni–O(1) ≈ 2.011(3) Å, Ni–O(2) ≈ 2.066(3) Å [11], Δ ≈ 0.055 Å and Cu–O(1) ≈ 1.964(3) Å, Cu–O(2) ≈ 2.010(3) Å [27], Δ ≈ 0.046 Å respectively, while in $Yb_2BaCoO_5$ they are Co–O(1) ≈ 1.998(23) Å and Co–O(2) ≈ 2.098(18) Å [3], with the distortion basal parameter Δ ≈ 0.100 Å being twice as large as for the other isostructural Ni and Cu oxides. It is note worthy that the M–O(2) bond length is always the longer of the two basal plane distances, which may be related to the fact that O(2) is closer than O(1) to the barium atoms.

On the other hand, in the isostructural *Pnma*-$R_2BaCuO_5$ phases it has been shown that the inter-pyramid oxygen–oxygen distance is the part of the structure that changes most on successive replacement of the rare earth atoms [27] and thus is the expected behaviour in the cobalt oxides, which will be confirmed by the high resolution neutron diffraction experiments that are now in progress in order to obtain a better accuracy in these interatomic distances.

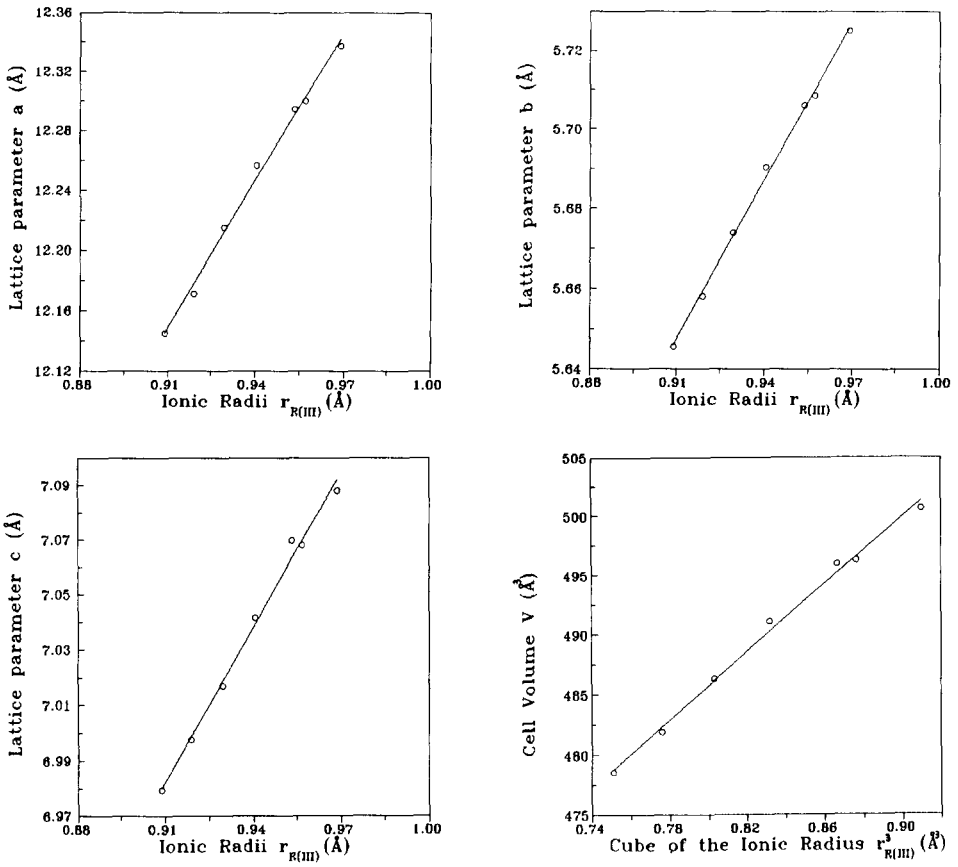


Fig. 3. Variation in lattice parameters and volume of unit cell *vs.* rare earth ionic radius.

### 3.2. *Magnetic properties*

In Figs. 4 and 5 the variation in $\chi$ *vs.* $T$ for the oxides $Y_2BaCoO_5$ and $Lu_2BaCoO_5$ respectively is shown. It can be observed that the susceptibility obeys a Curie–Weiss law over the whole measurement range and that the calculated magnetic moments of 5.0 and 4.9 BM for the yttrium and lutetium oxides respectively agree with the expected value for a high spin state of the $Co^{2+}$ free ion [30]. This result is quite different from that obtained in the isostructural $R_2BaCuO_5$ (R ≡ Lu and Y) and $Lu_2BaNiO_5$ oxides, where the existence of net maxima has been observed at very low temperatures, which is indicative of antiferromagnetic ordering in the copper [19–23, 31–33] and nickel [34] sublattices. This different magnetic behaviour may be due to the larger Co–O distances in the Co–O–R–O–Co pathways through which the antiferromagnetic interactions take place in comparison with the Cu–O and Ni–O bond lengths of the isostructural copper and nickel oxides. Moreover, the different electronic configuration of $Co^{2+}$ could be also very important in explaining the absence of interactions at low temperatures.

In the case of the remaining *Pnma*-$R_2BaCoO_5$ oxides (R ≡ Dy, Ho, Er, Tm and Yb) the magnetic behaviour should be more complex because of the coexistence of two paramagnetic cations $Co^{2+}$ and $R^{3+}$.

In all cases the magnetic susceptibility follows a Curie–Weiss law over a very wide temperature range. As was expected taking into account the crystal structure, both $Co^{2+}$ and $R^{3+}$ contribute to the magnetic susceptibility, and the magnetic moments given in Table 4 have been obtained after discounting the cobalt contribution by taking as reference the susceptibility of the $Y_2BaCoO_5$ oxide. Good agreement between the theoretical and observed magnetic moments for the various $R_2BaCoO_5$ oxides can be seen in Table 4. The negative values of the Weiss constant appear to indicate the existence of antiferromagnetic interactions at low temperature. However, only in the case of $Dy_2BaCoO_5$ has the presence of a maximum at 4.5 K in $\chi$ been observed (Fig. 6). Since the ground state of $Dy^{3+}$ is $^6H_{15/2}$ under the crystal field influence, the lowest starting level should be doubly degenerate and consequently, if cooperative interactions are not operative, the $\chi^{-1}$ *vs.* $T$ plot will show a downward deviation from linearity at low temperature. However, as can be observed in Fig. 6, an upward deviation is present, which confirms the presence of antiferromagnetism below 4.5 K. This assumption is also reinforced by the marked decrease

TABLE 2. Refined atomic coordinates and reliability factors (%) for the new *Pnma*-$R_2BaCoO_5$ oxides obtained from X-ray powder diffraction data

| Atom | Site | | $Dy_2BaCoO_5$ | $Er_2BaCoO_5$ | $Tm_2BaCoO_5$ | $Lu_2BaCoO_5$ |
|---|---|---|---|---|---|---|
| Ba | 4*c* | *x* | 0.903(1) | 0.901(1) | 0.901(1) | 0.902(1) |
| | | *y* | 0.25 | 0.25 | 0.25 | 0.25 |
| | | *z* | 0.920(1) | 0.924(1) | 0.924(1) | 0.923(1) |
| R(1) | 4*c* | *x* | 0.292(1) | 0.292(1) | 0.291(1) | 0.292(1) |
| | | *y* | 0.25 | 0.25 | 0.25 | 0.25 |
| | | *z* | 0.122(1) | 0.121(1) | 0.120(1) | 0.123(1) |
| R(2) | 4*c* | *x* | 0.074(1) | 0.074(1) | 0.073(1) | 0.074(1) |
| | | *y* | 0.25 | 0.25 | 0.25 | 0.25 |
| | | *z* | 0.400(1) | 0.400(1) | 0.401(1) | 0.399(1) |
| Co | 4*c* | *x* | 0.653(1) | 0.652(1) | 0.654(1) | 0.653(1) |
| | | *y* | 0.25 | 0.25 | 0.25 | 0.25 |
| | | *z* | 0.694(2) | 0.695(2) | 0.695(1) | 0.697(1) |
| O(1) | 8*d* | *x* | 0.435(3) | 0.435(2) | 0.435(2) | 0.436(2) |
| | | *y* | 0.993(5) | 0.994(4) | 0.992(4) | 0.995(4) |
| | | *z* | 0.168(4) | 0.169(3) | 0.170(3) | 0.172(3) |
| O(2) | 8*d* | *x* | 0.226(3) | 0.227(2) | 0.224(2) | 0.225(2) |
| | | *y* | 0.500(5) | 0.503(4) | 0.500(4) | 0.496(4) |
| | | *z* | 0.362(5) | 0.362(4) | 0.360(4) | 0.365(4) |
| O(3) | 4*c* | *x* | 0.100(4) | 0.098(3) | 0.099(3) | 0.103(3) |
| | | *y* | 0.25 | 0.25 | 0.25 | 0.25 |
| | | *z* | 0.074(5) | 0.072(4) | 0.075(5) | 0.072(5) |
| $R_p$ | | | 16.4 | 17.5 | 18.1 | 12.9 |
| $R_{wp}$ | | | 21.9 | 18.5 | 21.0 | 15.8 |
| $R_{exp}$ | | | 7.95 | 9.35 | 6.39 | 5.20 |
| $\chi^2$ | | | 7.57 | 3.92 | 10.8 | 9.20 |
| $R_b$ | | | 8.66 | 6.45 | 7.79 | 5.28 |

TABLE 3. Bond lengths M–O (Å) of the new *Pnma*-$R_2BaCoO_5$ oxides obtained from X-ray powder diffraction data

| M–O | $Dy_2BaCoO_5$ | $Er_2BaCoO_5$ | $Tm_2BaCoO_5$ | $Lu_2BaCoO_5$ |
|---|---|---|---|---|
| R(1)–O(1) (×2) | 2.32(3) | 2.30(2) | 2.30(3) | 2.29(2) |
| O(2) (×2) | 2.33(2) | 2.32(2) | 2.32(2) | 2.31(2) |
| O(2) (×2) | 2.37(2) | 2.36(2) | 2.35(2) | 2.33(2) |
| O(3) (×1) | 2.41(4) | 2.39(3) | 2.37(4) | 2.32(4) |
| R(2)–O(1) (×2) | 2.31(2) | 2.29(2) | 2.29(3) | 2.26(2) |
| O(1) (×2) | 2.36(2) | 2.35(2) | 2.34(2) | 2.32(2) |
| O(2) (×2) | 2.39(2) | 2.38(2) | 2.35(2) | 2.36(2) |
| O(3) (×1) | 2.34(3) | 2.33(3) | 2.31(4) | 2.31(3) |
| Ba–O(1) (×2) | 3.02(3) | 3.03(2) | 3.01(3) | 2.98(2) |
| O(1) (×2) | 3.29(2) | 3.24(2) | 3.22(2) | 3.20(2) |
| O(2) (×2) | 3.03(3) | 2.98(3) | 2.99(3) | 2.95(3) |
| O(2) (×2) | 2.93(2) | 2.91(2) | 2.88(3) | 2.89(2) |
| O(3) (×2) | 2.863(1) | 2.845(1) | 2.837(1) | 2.824(2) |
| O(3) (×1) | 2.65(4) | 2.63(3) | 2.64(4) | 2.62(4) |
| Co–O(1) (×2) | 2.02(3) | 2.00(3) | 1.99(3) | 1.98(2) |
| O(2) (×2) | 2.08(3) | 2.08(2) | 2.09(3) | 2.09(3) |
| O(3) (×1) | 2.00(4) | 1.99(3) | 2.01(4) | 1.97(4) |

observed in the $\chi T$ *vs.* $T$ plot (Fig. 6, inset), which shows a $\chi T$ value of only 5 e.m.u. mol$^{-1}$ K at 4.2 K.

Both $Er_2BaCoO_5$ and $Yb_2BaCoO_5$ show a similar magnetic behaviour (Figs. 7 and 8 respectively). Because of the half-integer value of $J$ in the ground state, the crystal field splits these ground terms, giving rise to downwards deviations from linearity in the $\chi^{-1}$ *vs.* $T$ plots at low temperature. This deviation is clearly

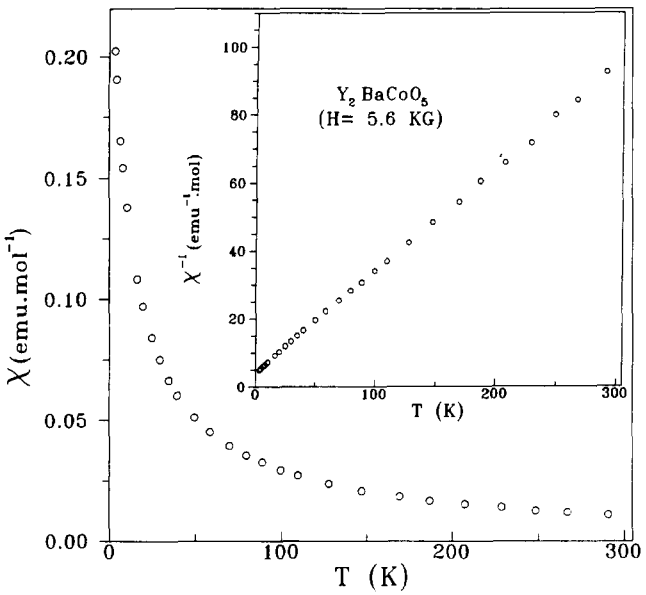


Fig. 4. Temperature dependence of the molar magnetic susceptibility for the $Y_2BaCoO_5$ oxide. The inset shows the $\chi^{-1}$ *vs.* $T$ plot.

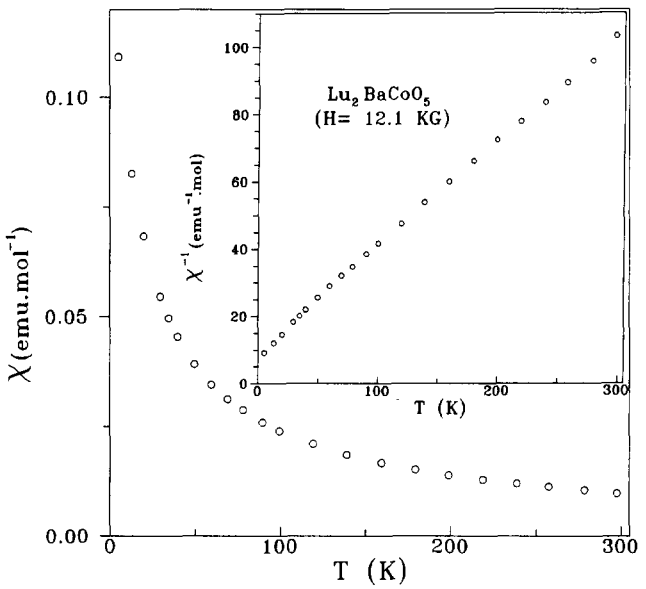


Fig. 5. Temperature dependence of the molar magnetic susceptibility for the $Lu_2BaCoO_5$ oxide. The inset shows the $\chi^{-1}$ *vs.* $T$ plot.

visualized in the case of $Yb_2BaCoO_5$ below 60 K, but the tendency breaks down at 10 K as can be observed in Fig. 8. Below this latter temperature the magnetic susceptibility decreases, probably owing to the operation of antiferromagnetic interactions in which both the $Co^{2+}$ and $Yb^{3+}$ sublattices appear to be involved.

In the case of $Ho_2BaCoO_5$ and $Tm_2BaCoO_5$ (Figs. 9 and 10 respectively) the deviation from Curie–Weiss behaviour is less marked than in the other oxides discussed above. This reflects the splitting of the $^5I_8$ and $^3H_6$ ground terms associated with $Ho^{3+}$ and $Tm^{3+}$ respectively under the influence of the crystal field. Although the negative values of the Weiss constant obtained for both oxides (Table 4) might be entirely due to the crystal field effect, the small values of $\chi T$ obtained at 4.2 K (9 and 5 e.m.u. mol$^{-1}$ K for the holmium and thulium oxides respectively) appear to indicate that somewhat antiferromagnetic interactions are operative at low temperature. This assumption has been fully confirmed recently by neutron diffraction experiments and the corresponding diffraction pattern obtained at 1.5 K shows the presence of high intensity magnetic reflections, indicating that both $Ho^{3+}$ and $Co^{2+}$ are involved in the interaction [35].

Neutron diffraction work is under way to confirm the assumption of three-dimensional antiferromagnetic ordering at low temperatures presented by these oxides and to determine the Néel temperatures.

TABLE 4. Experimental ($\mu_e$) and calculated ($\mu_c$) magnetic moments, Weiss constants ($\theta$) and temperatures at which the susceptibility is maximum ($T\chi_{max}$) for the *Pnma*-$R_2BaCoO_5$ oxides

| Compound | $\mu_e$ (BM) | $\mu_c$ (BM) | $\theta$ (K) | $T\chi_{max}$ (K) |
|---|---|---|---|---|
| $Dy_2BaCoO_5$ | 10.53[a] | 10.65 | −6.7 | 4.5 |
| $Ho_2BaCoO_5$ | 10.66[a] | 10.60 | −3.3 | – |
| $Er_2BaCoO_5$ | 9.51[a] | 9.59 | −5.4 | – |
| $Tm_2BaCoO_5$ | 7.50[a] | 7.57 | −7.3 | – |
| $Yb_2BaCoO_5$ | 4.58[a] | 4.54 | −18.6 | – |
| $Lu_2BaCoO_5$ | 4.88 | 0.00 | −21.0 | – |
| $Y_2BaCoO_5$ | 4.98 | 0.00 | −13.2 | – |

[a]Obtained taking into account the $Co^{2+}$ contribution.

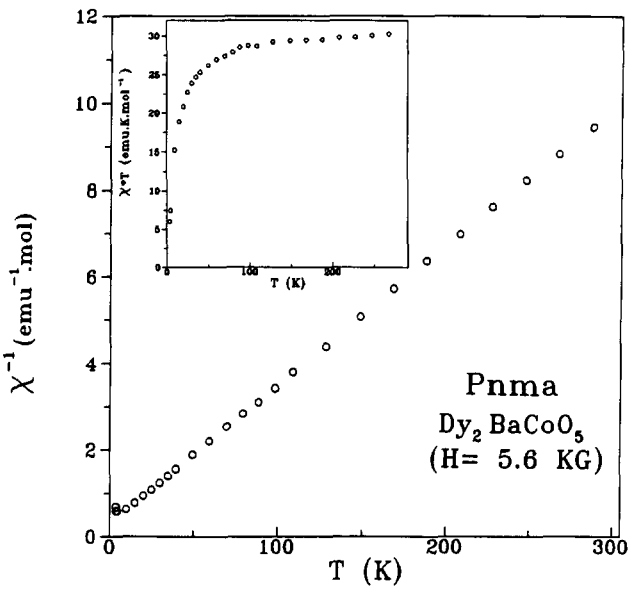


Fig. 6. Temperature dependence of the reciprocal molar magnetic susceptibility for the $Dy_2BaCoO_5$ oxide. The inset shows the $\chi T$ *vs.* $T$ plot.

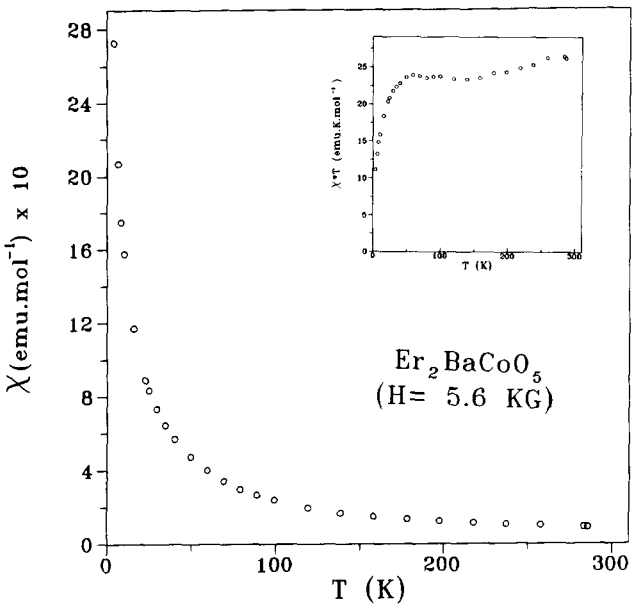


Fig. 7. Temperature dependence of the molar magnetic susceptibility for the $Er_2BaCoO_5$ oxide. The inset shows the $\chi T$ *vs.* $T$ plot.

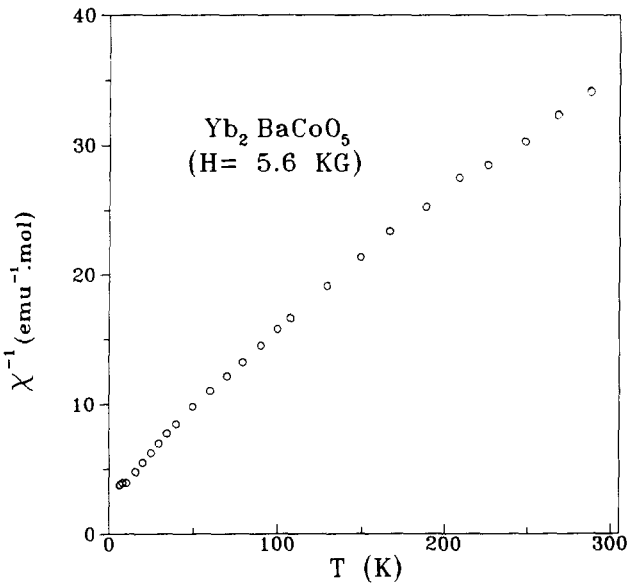


Fig. 8. Temperature dependence of the reciprocal molar magnetic susceptibility for the $Yb_2BaCoO_5$ oxide.

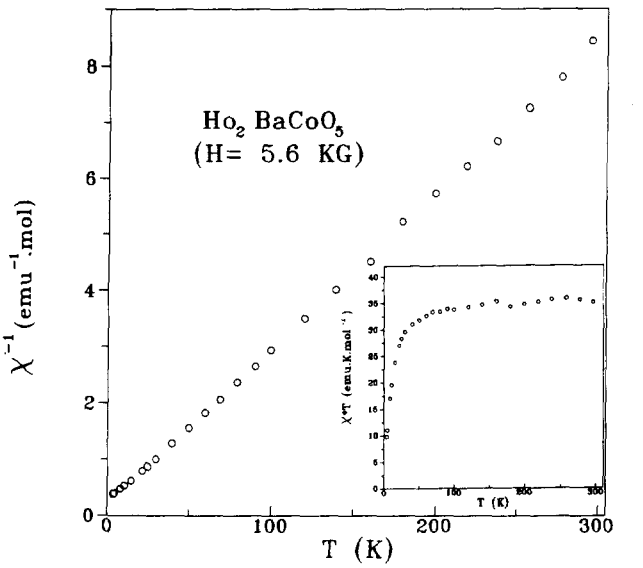


Fig. 9. Temperature dependence of the reciprocal molar magnetic susceptibility for the $Ho_2BaCoO_5$ oxide. The inset shows the $\chi T$ *vs.* $T$ plot.

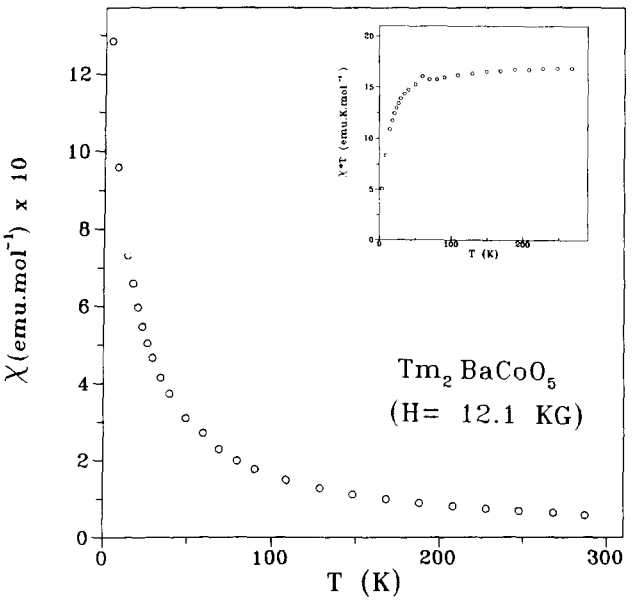


Fig. 10. Temperature dependence of the molar magnetic susceptibility for the $Tm_2BaCoO_5$ oxide. The inset shows the $\chi T$ *vs.* $T$ plot.

## Acknowledgment

We wish to thank the CICYT (Project MAT92-0374) for financial support.

## References

1 H. Mevs and Hk. Müller-Buschbaum, *Z. Anorg. Allg. Chem.*, *573* (1989) 128.

2 H. Mevs and Hk. Müller-Buschbaum, *J. Less-Common Met.*, *152* (1989) 139.

3 H. Mevs and Hk. Müller-Buschbaum, *Z. Anorg. Allg. Chem.*, *574* (1989) 172.

4 J. Hernández-Velasco, A. Salinas-Sánchez and R. Sáez-Puche, *J. Solid State Chem.*, in press

5 R. Sáez-Puche, F. Fernández and J. Hernández, *2nd Italian–Portuguese–Spanish Meeting in Inorganic Chemistry, Alfamar, March 1992,* Abstract IS 15.

6 E. Kluver and Hk. Müller-Buschbaum, *Z. Anorg. Allg. Chem.*, *619* (1993) 421.

7 R. Sáez-Puche, J. Hernández-Velasco and F. Fernández, *Solid State Ionics,* in press.

8 J. Hernández-Velasco and R. Sáez-Puche, *J. Alloys Comp., 198* (1993) 63.
9 A. Salinas-Sánchez, R. Sáez-Puche, J. Rodríguez-Carvajal and J.L. Martínez, *Solid State Commun., 78*(6) (1991) 481.
10 A. Salinas-Sánchez, R. Sáez-Puche, F. Fernández, A. Andrés, A. Lavat and E.J. Baran, *J. Solid State Chem., 99* (1992) 63.
11 E. García-Matres, J. Rodríguez-Carvajal, J.L. Martínez, J.A. Alonso, A. Salinas-Sánchez and R. Sáez-Puche, *Solid State Ionics,* in press.
12 E. García-Matres, J.L. Martínez, J. Rodríguez-Carvajal, J.A. Alonso, A. Salinas-Sánchez and R. Sáez-Puche, *J. Solid State Chem., 103* (1993) 322.
13 C. Michel and B. Raveau, *J. Solid State Chem., 43* (1982) 73.
14 S. Schiffler and Hk. Müller-Buschbaum, *Z. Anorg. Allg. Chem., 540–541* (1986) 243.
15 S. Schiffler and Hk. Müller-Buschbaum, *Monatsh. Chem., 117* (1986) 485.
16 R. Norrestam, M. Hjorth and J.O. Bovin, *Z. Kristallogr., 183* (1988) 245.
17 M.R. Wu, R.J. Ashburn, C.J. Torng, P.H. Hur, R.L. Mong, L. Gau, J. Huang, Y.Q. Wang and C.W. Chu, *Phys. Rev. Lett., 58*(9) (1987) 908.
18 H. Steinfink, J.S. Swinea, Z.T. Sui, H.M. Hsu and J.B. Goodenough, *J. Am. Chem. Soc., 109* (1987) 3348.
19 A. Salinas-Sánchez, R. Sáez-Puche and M.A. Alario-Franco, *J. Solid State Chem., 89* (1990) 361.
20 A. Salinas-Sánchez, R. Sáez-Puche and M.A. Alario-Franco, *Eur. J. Solid State Inorg. Chem., 28* (1991) 653.
21 R.Z. Levitin, B.V. Mill, V.V. Moshchalkov, N.A. Samarin, V.V. Snegirev and J. Zoubkova, *J. Magn. Magn. Mater., 90–91* (1990) 536.
22 R. Burriel, M. Castro, C. Pique, A. Salinas and R. Sáez-Puche, *J. Magn. Magn. Mater., 104–107* (1992) 619.
23 V.V. Moshchalkov, N.A. Samarin, I.O. Grishchenko, B.V. Mill and J. Zoubkova, *Solid State Commun., 78* (1991) 879.
24 J. Rodríguez-Carvajal, FULLPROF: a program for Rietveld refinement and pattern matching analysis, *Abstracts of Satellite Meeting on Powder Diffraction of XV Congr. of International Union of Crystallography, Toulouse, 1990,* p. 127.
25 L.N. Mulay and E.A. Boudreaux, *Theory and Applications of Molecular Paramagnetism,* Wiley, New York, 1976, p. 494.
26 R.D. Shannon and C.T. Prewitt, *Acta Crystallogr. B, 25* (1969) 925.
27 A. Salinas-Sánchez, J.L. García-Muñoz, J. Rodríguez-Carvajal, R. Sáez-Puche and J.L. Martínez, *J. Solid State Chem., 100* (1992) 201.
28 J.L. García-Muñoz, J. Rodríguez-Carvajal, X. Obradors, M. Vallet-Regi, J. González-Calbet and E. García, *Phys. Lett. A, 149* (1990) 319.
28 M.A. Beno, L. Soderholm, D.W. Capone, D.G. Hinks, J.D. Jorgensen, I.K. Schuller, C.U. Segre, K. Zhang and J.D. Grace, *Appl. Phys. Lett., 51* (1987) 57.
30 R.L. Carlin, *Magnetochemistry,* Springer, New York, 1986.
31 N.I. Agladze, G.G. Chepurko, M.N. Popova and E.P. Hlybov, *Phys. Lett. A, 133* (1988) 260.
32 I.V. Paukov, M.N. Popova and B.V. Mill, *Phys. Lett. A, 169* (1992) 301.
33 E.W. Ong, B.L. Ranakrishna and Z. Iqbal, *Solid State Commun., 60*(2) (1988) 171.
34 R. Sáez-Puche, J.M. Coronado, L.C. Otero-Díaz and J.M. Martín-Llorente, *Mater. Chem. Phys., 34* (1993) 233.
35 J. Hernández-Velasco, *Master Thesis,* Universidad Complutense de Madrid, 1992.